SOIL Discuss., 2, 955–994, 2015
www.soil-discuss.net/2/955/2015/
doi:10.5194/soild-2-955-2015

SOIL Discussions Open Access

Non-stationarity of electrical resistivity and soil moisture relationship in heterogeneous soil system: a case study

D. Michot[1], Z. Thomas[1], and I. Adam[1,2]

[1]AGROCAMPUS OUEST, UMR1069, Soil Agro and hydroSystem, 35000 Rennes, France
[2]Institut National de la Recherche Agronomique du Niger, Département Gestion des Ressources Naturelles, BP 429, Niamey, Niger

Received: 24 July 2015 – Accepted: 6 September 2015 – Published: 18 September 2015

Correspondence to: D. Michot (didier.michot@agrocampus-ouest.fr)

Published by Copernicus Publications on behalf of the European Geosciences Union.

Abstract

Root uptake is the most decisive key in water transfer involving soil and vegetation. It depends on water availability which can be evaluated by punctual measurements. Additionally, surface geophysical methods such as Electrical Resistivity Tomography (ERT) provide larger spatial scales. This paper focuses on investigating temporal and spatial soil moisture changes, along a toposequence crossed by a hedgerow, using ERT and punctual measurements. 10 ERT were performed over the studied period for a 28 m long transect and compared to matric potential and groundwater level measurements. Soil Volumetric Water Content (VWC) was predicted using two methods (i) from ER using Waxman and Smits model (ii) and from matric potential using experimental retention curve fitted by Van Genuchten model. Probability Density Functions (Pdfs) of our set of data show that the largest change, in mean values of ER as well as matric potential, was observed in the topsoil layer. We then analyzed the consistency between ER and punctual measurements in this layer by extracting the arrays in the junction between ER grids and punctual measurements. Pdfs of ER maps at each monitoring time (from T01 to T10) were also calculated to select the more contrasted distributions corresponding to the wettest (T06) and driest states (T10). Results of ER were consistent with matric potential measurements with two different behaviors for locations inside and outside the root zone. A strong correlation ($r = 0.9$) between VWC values from Waxman and Smits model and those obtained from retention curve was observed outside the root zone. The heterogeneous soil system inside the root zone shows a different pattern in this relationship. The shift in the relationship between ER and soil moisture for the locations outside and inside the root zone highlights the non-stationarity in heterogeneous soil system. Such systems were actually related to the high hedgerow root density and also to a particular topographical context (ditch and bank) which is encountered in Brittany and over north-west of Europe.

1 Introduction

Understanding the role of vegetation in the interface between the atmosphere and groundwater is the most decisive key for analyzing the processes involved in water transfer. The main impact of vegetation is root water uptake and hydraulic redistribution, which significantly modifies the processes involved in water transfer in the vadose zone. In Western Europe, hedgerow networks are a common and ancient tree alignment surrounding agricultural fields. Hedgerow removal due to farm enlargement is the major land use change after the Second World War. Previous studies suggest a significant impact of hedgerows on soil moisture (Caubel, 2001; Thomas et al., 2008) and rainfall distribution (Ghazavi et al., 2008). Many studies have explored the effect of hedgerows surrounding wetlands on water fluxes and the subsequent increase in transpiration (Thomas et al., 2012) and decrease in nitrate concentration (Grimaldi et al., 2009). The benefits of hedgerows in soil conservation have been highlighted by Walter et al. (2003). In agricultural landscapes throughout the world, combining trees and crops seems an appropriate alternative for providing the benefits of trees to crop requirements. Water availability can be monitored using direct and indirect soil moisture sensors. As significant spatial variability exists in the vadose zone, a dense array of sensors (e.g. tensiometers, TDR, piezometers) is usually required. However, a high density of sensors is not only expensive, but drilling to install them can disrupt hydraulic contact and induce preferential flow. Non-invasive geophysical imaging techniques, such as electrical resistivity tomography (ERT), might be an alternative way to monitor matric-potential distribution in the soil in relation to root water uptake. Specifically, ERT allows the spatial distribution of soil electrical resistivity (ER) to be mapped in 2-D or 3-D.

As a geophysical signal, ER is related to varying physical and chemical characteristics. ERT helps to identify spatial and temporal soil physical properties (e.g. structure, water content, fluid composition). Many applications of ERT have been developed over the last 20 years, from assessment of solute transport in aquifers (Muller el al.,

2010) to detection of soil salinity in irrigated zones (Adam et al., 2012). Samouëlian et al. (2005) reviewed ER as a function of soil properties, described the main electrical devices for 2-D or 3-D surveys and explained the basic principles of data interpretation. Soil ER mainly involves the constant physical properties of the soil, such as clay content, but also involves variable properties over time, such as soil water content, soil water electrical conductivity and temperature (Ward, 1990; Samouëlian et al., 2005). Thus, time-lapse ERT is an alternative way to monitor spatial and temporal water flux providing larger spatial scales. Numerous studies have tested the potential of ERT to monitor water flux processes, such as infiltration in unsaturated conditions (Descloitres et al., 2008; Al Hagrey and Michaelsen; Michot et al., 2001, 2003; Yamakawa et al., 2011; Zhou et al., 2001). Thus, in order to use ER to monitor VWC, it is necessary to perform a laboratory or field calibration (Michot, 2003), or to develop a pedotransfer function integrating data on soil properties (Hadzick et al., 2011; Brillante et al., 2014). Another alternative is to use a petro-physical model linking ER to VWC. There is various petro-physical models derived from Archie's law (1942) which were developed first for pure sand (without any clay). The empirical Waxman and Smits (1968) model based on Archie's law (1942) take into account the effect of clays on the resistivity and has been successfully applied in its simplified form on agricultural soils (Garré et al., 2011; Beff et al., 2013). Among five petro-physical models tested on a loamy soil to predict VWC and the soil bulk density in view or ERT application, the Waxman and Smits model appeared more consistent for electrical resistivity value $> 100\,\Omega$m (Laloy et al., 2011) which are often observed in dry soils. For lower ER values ($< 100\,\Omega$m), the volume-averaging method (Pride, 1994; Linde et al., 2006) outperformed the other tested models. A review of possible techniques to develop models that allow the use of ERT to spatialize soil water availability to plants was presented in Brillante et al. (2015). They describe methods and models to calibrate ER using TDR measurements.

Several authors have also described the distribution and biomass of tree roots using ERT (Amato et al., 2008, 2009; Zenone et al., 2008; Al Hagrey and Petersen, 2001; Rossi et al., 2011). Root presence in the soil is characterized by a highly resistive area

SOILD
2, 955–994, 2015

close to the tree trunk (Amato et al., 2008; Al Hagrey, 2007), and soil ER varies with root biomass density (Rossi et al., 2011). However, understanding the spatial heterogeneity of soil water content and the hydrological processes in a hedgerow landscape implies estimating the root water uptake of tree hedgerows. Werban et al. (2008) used ERT to monitor temporal changes in the distribution of soil water content in the root zone of a lupine plant in the laboratory. Garré et al. (2011) used ERT to measure soil water depletion caused by barley plants grown on an undisturbed soil monolith in a lysimeter. Michot et al. (2003) monitored soil water fluxes with ER imaging in an agricultural field after irrigation and detected preferential dryness just below cultivated maize plants. Similar observations of root zone drying, highlighted by an increase in ER, were shown in Mediterranean contexts by Al Hagrey (2007) and Nijland et al. (2010) on soils planted with cork oaks or covered by semi-natural vegetation of evergreen shrubs and trees. However, only Srayeddin and Doussan (2009) have quantified and mapped root water uptake of maize and sorghum in field conditions using time-lapse ERT. Recently, Garré et al. (2012) tested the ability of different ERT electrode arrays to detect soil moisture dynamics in a monocropping and an intercropping system. The most promising electrode array they tested was a combination of dipole-dipole and Wenner measurements. This effective electrode array was then tested for monitoring soil water dynamics in mixed cropping systems in the warm and humid tropical climate of Thailand (Garré et al., 2013). Most previous ERT work on soil water depletion induced by tree or plant root water uptake has focused on well-drained soils.

The present study had a double goal. Firstly, to investigate hedgerow roots effect on soil moisture using Electrical Resistivity Tomography (ERT) and punctual monitoring. Secondly, to verify the correlation between ER value and soil moisture in a heterogeneous soil system. Soil water depletion was estimated by punctual measurements of soil matric potential over the studied period. ER values were converted to soil volumetric content (VWC) using the Waxman and Smits petro-physical model. VWC values were compared to those obtained from matric potential using retention curve. Our case study focused on a toposequence located in a hillslope where the hydrology was controlled by shallow groundwater. The toposequence was located in a bottomland crossed by a hedgerow. The hydrological year was particularly wet.

2 Materials and methods

2.1 Study site

The study site was located in Brittany, western France. Hillslope hydrology was controlled by shallow groundwater developed in schist bedrock with silt loam soils. An oak hedgerow (*Quercus robur*) running north-to-south, planted perpendicular to the slope, created a clear barrier between two contrasting zones. Upslope of the hedgerow, the only land use was well-drained hillslope soils with permanent pasture. Downslope of the hedgerow was a bottomland with waterlogged soils and both permanent pasture and wet-meadow vegetation (*Carex* spp.). A 28-m soil transect perpendicular to the hedgerow was established from 16 m upslope of the hedgerow (UP16) to 12 m downslope (DW12). The mean slope was 4.8 and 11.8 %, respectively, on the transect upslope and downslope of the hedgerow. The difference in elevation between UP16 and DW12 was about 2 m (Fig. 1). In the study site, the wetland extended from 10 m downslope the hedgerow to the stream.

Long-term (32-year mean) annual rainfall (R) at a nearby weather station (Le Rheu, 5 km from the study site) was $\sim$720 mm, annual potential evapotranspiration (PET-Penmann) was $\sim$650 mm, and annual air temperature was $\sim$11.7 °C, ranging from 5.4 °C in January to 18.4 °C in August (Ferren, 2004). During the studied period, rainfall and PET data were collected at the Saint-Jacques meteorological station (48°4′12″ N, 1°43′36″ W), 5 km from the study site.

2.2 Soil properties

The organization and geometry of soil horizons was described in 2-D vertical cross section in a trench of 2 m deep and 28 m long that was excavated parallel to the transect

SOILD
2, 955–994, 2015

(Fig. 1). Soils and horizons were identified according to the World Reference Base of Soil Resources (FAO, 2006). Soil texture, bulk density and hydraulic conductivity were measured at seven locations along the transect (Fig. 1) where the soil matric potential (Ψ) and groundwater level (GWL) were monitored i.e. at 16, 8, 4 and 1 m upslope (UP16, UP8, UP4 and UP01) and 2, 6, 12 m downslope (DW2, DW6 and DW12).

We observed a luvic and stagnic Cambisol and a stagnic Fluvisol respectively from upslope to downslope. In the upslope zone, the thickness of the organo-mineral loamy A horizon increased from 0.4 to 1.1 m from upslope to the ditch close to the hedgerow (Fig. 1). In the downslope zone, the organo-mineral A horizon was thinner and ranged from 0.1 m below the hedgerow to 0.5 m at the boundary with the epistagnic fluvic horizon (B1 horizon, see Fig. 1) of the wetland.

Soil horizon organization differed slightly below the hedgerow, particularly under the ditch and in the soil bank (Fig. 1). In the studied hillslope, a ditch was parallel to the hedgerow. Soil thickness above the weathered schist bedrock varied greatly. It ranged from 1.3–1.6 m near the hedgerow in the upslope zone to less than 0.9 m in the downslope zone. Redoximorphic features appeared below a depth of 0.5 m in the upslope zone and began at the topsoil surface in the downslope zone. The clay content of shallow and organo-mineral horizons ranged from 14.6–16.0 % in the upslope zone and exceeded 20 % in the downslope zone (Fig. S1 in the Supplement). At greater depths, the endostagnic B horizon observed in the luvic Cambisol (UP16) had a clay content of 23.3 %, but the highest clay content was observed in the stagnic Fluvisol in the bottomland (DW12). It ranged from 24.7 % in the shallow epistagnic fluvic B1 horizon to 27.1 % in the endostagnic fluvic B2 horizon at depths of 0.4 to 0.9 m. At depth, the schist saprolite (C mineral horizon) had a loam-sandy-clayey texture (Figs. 1 and S1). We observed several coarse particle accumulations (e.g. stones, quartz veins) in the 2-D vertical soil cross section, in particular in the upslope zone and near the ditch along the hedgerow.

As expected, soil bulk density increased with soil depth at all distances along the transect (Fig. S2a and b in the Supplement). Vertically, variability in bulk density in the

SOILD
2, 955–994, 2015

upslope zone was lower than that in the downslope zone. Horizontally, in the upslope zone, soil bulk density increased with distance from the hedgerow, respectively, from 1.3 (UP04) to 1.6 (UP16) at 5 cm deep and from 1.5 (UP04) to 1.7 (UP16) at 100 cm deep (Fig. S2a and b in the Supplement). Additionally, bulk density was higher in the topsoil layer (A horizon) in the upslope versus downslope zone.

Soil hydraulic conductivity was measured at conditions of near saturation, i.e. at a low water potential of −0.05 kPa, with a Decagon 4.5-cm diameter mini disk infiltrometer (Decagon Devices, 2006). Soil hydraulic conductivity was determined from steady-state flux data according to the Wooding (1968) approach. Multiple depths were measured at each monitored location along the toposequence (Fig. S2c and d in the Supplement). As a function of changes in bulk density, hydraulic conductivity at −0.5 hPa water potential ($K_{(-0.5\,\mathrm{hPa})}$) decreased with increasing soil depth at all locations along the transect except for DW2 where a singular point was observed at 60 cm depth. Mean $K_{(-0.5\,\mathrm{hPa})}$ values were significantly higher in the downslope zone (6×10^{-4}, 5.7×10^{-4} and 5.5×10^{-4} m s^{-1} at DW2, DW6 and DW12, respectively) versus the upslope zone, especially in the topsoil i.e. depth > 50 cm (200×10^{-6} m s^{-1} at UP4, UP8 and UP16). $K_{(-0.5\,\mathrm{hPa})}$ values (Fig. S2 in the Supplement) were relatively homogeneous in the vertical plane upslope the hedgerow; while a difference of two orders of magnitude was observed between the topsoil and subsoil in the downslope zone. A lower K and higher bulk density are well-known characteristics of bottomland soils.

The soil surface occupied by roots along the trench was estimated using a quadrat of 1 m^2 subdivided into 100 squares of 100 cm^2 each (Breda et al., 1995). First, the quadrat was located from 10 to 110 cm depth to ovoid counting pasture roots in the top layer. Otherwise, roots without woody structure were not considered. For each 100 cm^2 square only the woody roots were counted and summed for 1 m^2 section of the trench, both upslope and downslope, and the percentage of total woody roots that occurred in each section was calculated as presented on Ghazavi et al. (2008). Along the transect, vertical root distribution within each 1 m was also calculated at four depth classes: 10–50, 50–100, 100–150, and 150–200 cm (Fig. S2e and f in the Supplement). According

SOILD
2, 955–994, 2015

Title Page
Abstract | Introduction
Conclusions | References
Tables | Figures
◀| |▶
◀ ▶
Back | Close
Full Screen / Esc
Printer-friendly Version
Interactive Discussion

to the observations of Ghazavi et al. (2008), horizontal distribution of tree roots in the upslope and downslope zones was asymmetric, with 76 % of tree roots located upslope and only 24 % of roots located downslope. Vertically, tree roots reached deeper in the upslope zone than in the downslope zone. Moreover, in the upslope zone, 61, 36, 3 % of roots were, respectively, located 10–50, 50–100, and 100–200 cm deep. In the downslope zone, 92 % of roots were located 10–50 cm deep, and only 8 % were 50–100 cm deep.

2.3 Hydrological monitoring: punctual measurements

Soil matric potential and groundwater level were monitored as described by Ghazavi et al. (2008, 2011). Seven locations were monitored continuously with one piezometer and five tensiometers each (Fig. 1). Three piezometers were located at 16, 8 and 4 m upslope of the hedgerow, each with a tube diameter of 11.2 cm and a total length of 7.5 m, of which 4 m at its base were screened. The other four piezometers were located at 1 m upslope and 2, 6 and 12 m downslope of the hedgerow, each with a diameter of 6.8 cm and a total length of 4.5 m, of which 2 m at its base were screened. For each monitored location, five tensiometers were installed at depths of 25, 50, 100, 150, and 200 cm. The vertical soil matric-potential gradient was used to interpret the ER. 10 monitoring times from 10 March to 13 August 2007 are called T01 to T10.

2.4 Electrical resistivity monitoring

2.4.1 Timeframe ERT

Temporal monitoring of ER along a 2-D cross section (Fig. 1) was performed for 10 monitoring times (T01 to T10). Resistivity was measured with a Syscal R1 resistivity meter (Iris Instruments, Orléans, France). The precision of its intensity and voltage was ± 0.3 % which is consistent with measurements taken under constant surface conditions. The experimental design included a row of 64 electrodes that were lined up on the soil surface perpendicular to the hedgerow (Fig. 1). With an electrode spacing of 0.5 m, the experimental device measured 31.5 m long. The electrodes remained on the soil surface during the entire experiment to avoid changes in electrode polarization and ensure high-quality measurements. The resistivimeter followed a pre-programmed measurement sequence, and a multiplexer switched among the electrodes.

A dipole-dipole arrangement was chosen because it allowed the greatest number of measurements for the number of electrodes present, which was advantageous for data inversion. Moreover, the dipole-dipole array was highly sensitive to horizontal changes in resistivity but relatively insensitive to vertical changes. For each resistivity measurement, an electrical current was passed between two adjacent electrodes (dipole AB), and the potential difference was measured between two other neighboring electrodes (dipole MN). The bulk ER ρ_a of a half-space measured with a dipole-dipole electrode array is:

$$\rho_a = 2\pi \frac{\Delta V}{I} \frac{1}{(1/\mathrm{MA} - 1/\mathrm{MB} + 1/\mathrm{NB} - 1/\mathrm{NA})} = k\frac{\Delta V}{I} \quad (1)$$

Where I is the intensity of the current passed between electrodes A and B, ΔV is the potential difference measured between electrodes M and N, and k is the "geometric factor", whose value depends on the type of array. For a dipole-dipole array, k is calculated as:

$$k = \pi (n \cdot (n+1) \cdot (n+2) \cdot a) \quad (2)$$

Where a is the spacing (distance, in m) between electrodes of each dipole, and n is a dipole-separation factor whose value is usually an integer multiple of the distance between the current or potential electrode pair. To obtain the necessary resolution, 646 measurements were taken during each ERT. Measurements were located at 12 pseudodepths of investigation, the first 5 with a of 0.5 m and n of 1, 2, 3, 4 and 6. Since the potential measured between M and N decreases rapidly with increasing n, it is not advisable for n to exceed 6. To maintain measurement quality at greater depths, which

SOILD
2, 955–994, 2015

Non-stationarity of electrical resistivity and soil moisture relationship

D. Michot et al.

have high signal-to-noise ratios, three pseudodepths were investigated with *a* of 1 m and *n* of 2, 3 and 4. The remaining four pseudodepths had *a* of 1.5 m and *n* of 2, 3, 4 and 5. In a dipole-dipole electrode setup, the spacing between the dipole that passes the current and the dipole that measures the potential difference is gradually increased. By convention, bulk ER measurements are represented at the centre of the quadripole and at a depth proportional to the spacing between dipoles. Each ERT required 1 h and 40 min.

2.4.2 ERT data processing

Inverting resistivity measurements is an essential step before interpreting them because the raw resistivity measurements rarely reveal the true structure of the soil. Thus, resistivity sections were inverted with the software RES2DINV (Loke and Barker, 1996) using a smoothness-constrained least-square method to produce a 2-D subsurface model. In the first iteration, a homogeneous earth model was used as a starting point from which partial derivative values of resistivity could be calculated analytically. For subsequent iterations, a quasi-Newton method was used to estimate the partial derivatives, which reduced computing time. In this method, Jacobian matrices for the homogeneous earth model were used for the first iteration, and those of subsequent iterations were estimated with an updating technique. The model consisted of a rectangular grid. Software determined the resistivity of each mesh, which calculated the ER of each section according to field measurements. An iterative optimization method consisting on minimizing the difference between measured resistivity values and those calculated with the inversion model by minimizing the root mean square error (RMSE). Topographic correction was applied to this inversion process. The grid obtained (Fig. S3 in the Supplement) was composed of rectangular meshes defined by their corner coordinates. Each ERT was inverted independently, considering the same number of measurements. Further details about inversion methods are available in the literature (Loke and Barker, 1996).

SOILD
2, 955–994, 2015

Bulk ER of unsaturated soils decreases when water content increase, and vice versa (Ward, 1990). In saturated zones, changes in bulk ER are usually linked to changes in groundwater electrical conductivity.

During the monitoring period, soil drying due to evapotranspiration was analyzed using statistics of each ER map. A probability density function (Pdf) of the map at each monitoring time (T01 to T10) was calculated, and Pdfs were compared to select the more contrasted distributions. The lowest ER mean represents the wettest state (initial state), while the highest ER mean represents the driest state (final state). The change in ER was calculated between initial and final states and was compared to that in matric potential for the same states.

2.4.3 ER conversion to VWC

To quantify the relationship between ER and matric potential, ERs values were extracted at the location of each tensiometer (red circles in Fig. S3 in the Supplement). ER and matric potential of the topsoil layer (25 and 50 cm depth) corresponding to the unsaturated zone were analyzed. ER values were also converted to soil volumetric water content (VWC) from the Waxman and Smits (WS) model (Waxman and Smits, 1968) simplified by Garré et al. (2011, 2013) using Eq. (3).

$$\mathrm{SWC} = \left\{ \frac{\left[\frac{1}{\mathrm{ER}} - b\right]}{a} \right\}^{1/n} \tag{3}$$

Where a (S m^{-1}), b (S m^{-1}), and n are fitting parameters. As explained by Garré et al. (2011), those parameters could be explained in a physical way in combination with the porosity: a is related to the pore water conductivity and b is related to the soil surface conductivity. The parameter n is related to pore connectivity in the full Waxman and Smits model.

As the variation range of Waxman and Smits parameters is unknown on the studied toposequence, a sensitivity analysis was performed using the range of the parame-

SOILD
2, 955–994, 2015

ters proposed by Garré et al. (2011). In this study, four horizons of an orthic Luvisol developed in a Loess parent material from Germany were studied. In term of pedogenesis and texture, orthic Luvisol is relatively closed to those observed in our studied toposequence, especially in the upslope zone. For each parameter of Waxman and Smits model 3 values (Table 1) were tested leading to 27 simulations. VWC values were calculated for each extracted cell grid.

Using the retention curves from Ghazavi et al. (2011), measured on the soil horizons of this studied toposequence, we also convert the soil matric potential data into VWC. Experimental retention curves (Fig. S5 in the Supplement) were fitted using Van Genuchten model (Van Genuchten, 1980) from the Eq. (4).

$$\theta(h) = \begin{cases} \theta_r + \dfrac{[\theta_s - \theta_r]}{\left\lfloor 1 + |\alpha . h|^n \right\rfloor^m} \text{ for } h < 0 \\ \theta_s \text{ for } h \geq 0 \end{cases} \quad (4)$$

Where θ, volumetric water content (VWC [$cm^3 cm^{-3}$]); "s" for saturated, "r" for residual; "h", pressure head or matric potential [hPa]; α, n and m are Van Genuchten parameters with $m = 1 - 1/n$.

The Van Genuchten parameters are presented Table S1.

3 Results

3.1 Rainfall and Penmann PET

Cumulative rainfall and PET-Penmann were calculated between each monitoring time (T01 to T10). During the monitoring period, net rainfall (Rainfall-PET) of each interval between ERTs was higher than that during the same period of the previous 6 years (2001–2006) (Fig. 2). Also, the lowest net rainfall measured between ERTs during the monitoring period was about −40 mm, compared to −150 mm observed during the previous 6 years. Thus, the hydrological year studied was particularly wet.

3.2 ER sections and statistical distribution of ER

Probability density functions (Pdfs) of ER at each measurement time (from T01 to T10) were Gaussian and similar to each other except T10 (Fig. 3). T06 and T10 had the greatest differences in ER value statistics (see Table 1) and were selected respectively as wet and dry states. To ovoid redundancy, we describe only ER maps of T06 and T10. At both dates, a superficial layer from 0–0.80 m deep in the upslope zone with 100–200 Ωm of ER. In the downslope zone, a small localized resistive structure appeared at a distance of 1–2 m from the hedgerow. In the upslope zone a resistive layer was formed by the unsaturated well-drained organo-mineral A horizons (Fig. 4). Below this resistive layer, a conductive one was observed with 20–60 Ωm of ER. The thickness of this conductive structure decreased and reached the ground surface from 4–12 m downslope the hedgerow and show a vertical conductive structure below the hedgerow. A third layer with resistivity ranged from 60 to > 200 Ωm was observed deeply (< −2 m) in the upslope zone and was shallow downslope the hedgerow with a slightly variable along the slope (Fig. 4). Over the studied period, a discontinuity in this layer between upslope and downslope zones appears vertically below the hedgerow where the lowest resistivity (< 20 Ω m) was observed (dark blue in Fig. 4). Local resistive structures (> 150 Ωm) observed at the cross-section boundaries, below the ditch and at DW12. Such local anomalies were probably due to inversion method artefacts.

3.3 Time-frame ERT and matric potential profiles

The map of percentage change in electrical resistivity highlights temporal changes in ER between wet (T06) and dry (T10) states (Fig. 5). This map was compared to matric potential profiles measured for each location at T06 (dash lines in Fig. 5) and T10 (solid lines in Fig. 5). The map of Fig. 5 and punctual measurements highlight two main areas with large differences in ER. From 16 m upslope to 7 m downslope along the toposequence, an increase in ER by 20–100 % in the topsoil (0–0.9 m deep) (Fig. 5). In contrast, ER of the subsoil (> 1 m) increased by approximately 20 %, with multiple localized structures in which ER decreased by 20–80 %. Below the hedgerow, ER increased in a three-pronged pattern, with the upslope branch turning down toward the ditch at 45°, a vertical branch extending beneath the tree, and the downslope branch following the soil surface. Changes in ER were negative from 7–13 m downslope, but the highest decrease in ER (−80 %) was observed 1–4 m upslope below a depth of 2 m. Changes in soil matric potential corresponded to changes in ER (Figs. 5 and S4). According to matric potential data, the topsoil layer was drier (at depths of 0.25 and 0.5 m) than the subsoil (at depths of 1, 1.5 and 2 m). Soil matric potential decreased upslope at a depth of 0.5 m: from −20 to −152 hPa at 16 m, −127 to −615 hPa at 8 m and −75 to −425 hPa at 4 m. Under the ditch 1 m upslope and 2 m downslope, the change in soil matric potential confirmed soil drying down to, respectively, 1 and 0.5 m. The soil was unsaturated to a depth of 0.40 m at 6 m downslope. Moreover, even though the soil was saturated by groundwater, electrical resistivity of several localized structures increased by 5–80 % (Fig. 5). These structures were located mainly from 9–11 and 1–3 m upslope and 1.5–4 and 11–13 m downslope.

Pdf of ER (Fig. 6a) highlights the shift in the mean value between the whole domain and the topsoil layer as were the mean values of matric potential Pdf (Fig. 6b). For the top soil layer, the mean value of ER was highest when matric potential mean value was lowest corresponding to a driest soil for the wet as well as for the dry states. The difference in ER between the whole domain and the topsoil layer was about 26 Ωm for T06 (wet state) and reaches 110 Ωm for T10 (Fig. 6a). For matric potential the difference between the whole domain and the topsoil layer was about −73 hPa for T06 and −200 hPa for T10 (Fig. 6b). The greatest changes in both ER and matric potential were located in the topsoil. In the topsoil layer, change in mean ER and matric potential between the wet and the dry state was respectively about 120.5 Ωm and −277 hPa (Fig. 6a and b). Pdfs of ER as were Pdfs of matric potential show the same shape between the wet (T06) and dry (T10) state with an increase in data dispersion through a highest amplitude for the dry state (Fig. 6).

3.4 Comparison of punctual measurements: matric potential versus ER

In the unsaturated topsoil, punctual measurements of matric potential were consistent with ER value extracted for each grid (Fig. 7). Two behaviors were observed for the locations inside and outside the root zone (Fig. 7). According to the root system pattern (Fig. S2e and f in the Supplement), we assume that UP16, UP8 and DW12 are not influenced by the root system. It will be considered as an outside root zone. The locations inside the root zone were UP4, UP1, DW2 and DW6. For the locations inside (grey circles in Fig. 7) and outside (red circles in Fig. 7) the root zone two different patterns in the relationship between ER and matric potential were observed. Outside the root zone, a linear relationship was observed ($r^2 = 0.8$) whereas a dispersion in this relationship appears for the measurements inside the root zone ($r^2 = 0.3$). We also observed that matric potential range measured outside the root zone remains in the same order of magnitude for both wet and dry states. The two states which are the wet (full circles representing T01 to T06 in Fig. 7) and the dry (open circles representing T07 to T10 in Fig. 7) were analyzed separately.

Upslope, the location situated at 4m from the hedgerow (UP4) shows a similar pattern as the locations outside the root zone during the wet state (red square in Fig. 7). UP4 switch to the pattern of the locations inside the root zone during the dry state (grey square in Fig. 7).

3.5 VWC estimation

Figure 8 shows relationship between ER and VWC obtained from Waxman and Smits model (black circles) with a standard deviation corresponding to the set of Waxman and Smits parameters. The range of variation in VWC prediction from Waxman and Smits model was highest for small ER values (< 75 Ωm). Outside the root zone (red circles in Fig. 8), VWC values predicted from retention curve were consistent with VWC from Waxman and Smits model both for wet (Fig. 8a) and dry state (Fig. 8b). Inside the root zone (grey circles in Fig. 8), VWC values predicted from retention curve were smaller

SOILD
2, 955–994, 2015

than VWC from Waxman and Smits model except for the location UP4 during the wet state (red square in Fig. 8a). For this location, VWC predicted from retention curve was slightly smaller than Waxman and Smits prediction during the dry state (grey square in Fig. 8b).

Figure 9 shows the relationship between VWC estimated from retention curve and VWC from Waxman and Smits model. Red and grey circles show respectively the locations outside and inside the root zone. The two states which are the wet (full circles representing T01 to T06 in Fig. 9) and the dry (open circles representing T07 to T10 in Fig. 9) were analyzed separately. For the wet as well as the dry state, the relationship between the two predictions shows a strong correlation ($r = 0.9$) for the locations outside the root zone. We observed that the location UP4 fit quite good especially for the wet state (red square in Fig. 9). During the dry state the relationship between the 2 predictions remain acceptable with a smaller VWC from retention curve (grey square in Fig. 9). A shift between the locations inside and outside the root zone indicates two different patterns. VWC values predicted from Waxman and Smits model show highest soil moisture for the location inside the root zone (both full and open grey circles in Fig. 9).

4 Discussion

VWC prediction from ERT becomes a classical approach widely used by geophysicists. The methodology that we developed in our study was summarized Fig. 10 indicating the steps from data acquisition to processing. ER changes over time were performed without removing the effect of soil temperature variations over studied period as such data were missed. Pdfs of ER and matric potential were helpful for analyzing statistical range of data and selecting the relevant monitoring time. The more contrasted times corresponding to the wet (T06) and dry period (T10) were analyzed. The ER and matric potential data from the unsaturated zone were extracted to analyze the relationship between ER and matric potential (Fig. 10). The simplified petro-physical model of Waxman and Smits was then used to convert ER data to VWC. VWC was also predicted using retention curves (Fig. 10).

4.1 Soil properties and horizons organization

Vertically, ER maps revealed three main structures along the toposequence: (i) a resistive topsoil layer (red and yellow in Fig. 4) underlying the well-drained organo-mineral A horizon in the upslope zone, (ii) stagnic (A) and endostagnic (E, B) horizons that are more conductive (blue cyan in Fig. 4), (iii) deep C mineral horizon with intermediate ER (from green to red in Fig. 4) and irregular structures that were probably related to the degree of weathering of the Brioverian schist.

The three main structures are crossed by a vertical conductive structure, below the hedgerow (blue cyan in Fig. 4). We hypothesized that this structure may result from a higher degree of bedrock weathering caused by the main taproot (Baffet, 1984). Clay content increase with bedrock weathering inducing ER decrease at the vertical conductive structure. At the taproot proximity, water preferential flow participates also to the bedrock weathering.

As expected, our results show that lateral and vertical changes in ER are consistent with clay content measurements at multiple depths (Ward, 1990). In the downslope zone, clay content is 4–6 % higher than upslope zone (Fig. S1 in the Supplement). In addition, clay content increases and ER decrease with depth for all upslope locations (UP16, UP8, and UP4). ER also decreased when soil bulk density increased from the topsoil to the depth of the unsaturated zone (Fig. S2a and b). Besson et al. (2004) obtained similar results, indicating that soil ER was sensitive to bulk density. An increase in bulk density from 1.39 to 1.59 in a loamy soil corresponded to an 11 Ωm decrease in ER (Besson et al., 2004).

For the 10 ER maps, the most conductive layer, with an ER of 20–60 Ωm (Fig. 4), was located at the groundwater level and reached the surface in the downslope zone. The most conductive layer was related to the combined effect of: (i) shallow groundwater

SOILD
2, 955–994, 2015

rising to ground level from the wetland, (ii) low bulk density and (iii) high hydraulic conductivity increasing infiltration rate.

4.2 Spatial distribution of hedgerow roots in the unsaturated zone

Most roots were located in the upslope zone from 0.1–1.0 m deep (61 % from 0.1–0.5 m deep and 36 % from 0.5–1.0 m deep) and extended up to 6 m upslope from the hedgerow (Fig. S2e and f). Downslope, 92 % of roots were located from 0.1–0.5 m deep and only 8 % were located from 0.5–1.0 m deep (Fig. S2e and f). In addition, oak roots did not extend further than 9 m downslope. The temporal change in ER was largest in the topsoil layer and inside the root zone. The ER changes and punctual matric potential measurements between T06 and T10, after a long dry state (21 days with $R-\text{PET}=-25$ mm) (Fig. 2b), show gradual soil drying (see Fig. 5). Matric potential maps and gradients show a drier zone inside the root zone (Fig. S4b in the Supplement) highlighting water flux toward the hedgerow. These gradients were induced by root water uptake and agree with the literature on the spatial distribution of oak root systems (Drénou, 2006; Lucot, 1994). According to Drénou (2006), oak root (*Quercus robur*) exploration begins at the bottom of the trunk, and a mean of seven lateral roots (or branch roots) forms the frame of the surface root system. Generally, the surface lateral roots are spaced at a 30–60° angle from each other, and each forks at a mean radius of 0.5 m to produce two roots. Thus, a mean total of 14 lateral roots are present, with the potential to colonize the soil more than 20 m from the tree without reaching deeper than 0.6 m. A second level of horizontal roots appears under the previous ring of roots, but none of these roots exceeds 3 m in length. The primary oak taproot develops secondary oblique taproots, while the horizontal roots from the second level produce several secondary vertical taproots. These taproots branch out and fill soil at depths of 0.9–1.5 m when there is no obstacle. In our study, the spatial distribution of the root system was influenced by soil characteristics and anthropogenic features such as the ditch and the embankment on which the hedgerow was planted. Investigation of root depth along the toposequence was limited by a compact soil layer with a high bulk density of 1.6 (Fig. 4b in the Supplement) starting at a depth of 0.6 m.

In agreement with previous observations (Amato et al., 2008; Al Hagrey, 2007; Rossi et al., 2011), our results show several highly resistive areas close to the tree trunk (Fig. 4). Increases in ER between the wet and dry states (Fig. 5) likely identify the spatial limits of the hedgerow root system highlighting a three-pronged pattern inside the root zone. Rossi et al. (2011) demonstrated that ER variability in an orchard was related only to root biomass density. In our experiment, a quantitative analysis of the relationship between ER and root density was not relevant as the transects used were not exactly the same.

4.3 Consistency between ER and matric potential

Changes in ER are related to parameters such as volumetric water content, solute concentration and temperature (Ward, 1990). According to our experimental design, changes in ER were compared to those in soil matric potential, which were converted into volumetric water content by using measured retention curve (Sect. 4.4).

Two different behaviors in the relationship between ER and matric potential were observed between the locations outside the root zone (UP16, UP8, and DW12) and those inside the root zone (UP4, UP1, DW2 and DW6) with an r^2 of 0.8 and 0.3 respectively (Fig. 7). However, for the location UP4, this relationship adequately fit the curve obtained outside the root zone during the wet state (T01–T06). Despite of a high root density, the location UP4, showed the same behavior as the locations outside the root zone. Wet and leafless period which occurred from the autumn to the beginning of spring without transpiration (Thomas et al., 2012) was characterized by a non-influence of the root system. ER value show this non-influence for UP4 during this period. UP4 shifted to the relation of the locations inside the root zone during the dry state. For all the locations inside the root zone, we also identified distinct differences in the relationship between ER and matric potential between wet and dry state. Inside the root zone, the relationship between matric potential and ER has a high variability from wet to dry states probably caused by soil heterogeneities (Fig. 7). A decrease in matric potential (from −100 to −650 hPa) inside the root zone was related to a small change in ER. In our study site, the hedgerow with a bank and a ditch increased soil variability (Fig. 1). Moreover as described by Hesse (1990), variation in topography modifies bulk electrical resistivity measurements for a given electrodes array. For a homogenous soil system, bulk electrical resistivity decreases over a bank and increases over a ditch (Hesse, 1990). Topographical singularities creates ER value anomalies.

The ability of ER to predict soil matric potential was quite good along the toposequence outside the root zone (Fig. 7). We hypothesized that the numerous singularities around the hedgerow combined to the high root density increased the signal-to-noise ratio. Considering the shift in the mean value of ER distribution (Pdf in Fig. 6) between the initial (T06) and final state (T10), the decrease in matric potential did not change the shape of ER distribution but only their mean value, which was highest when the soil was drier. During the dry state, matric potential maps (Fig. S4b in the Supplement) showed a drier zone inside the root zone with matric-potential gradients indicating water flux toward the hedgerow.

4.4 VWC prediction using ER inside and outside the root zone

By analyzing 27 simulations from Waxman and Smits model, our results highlight the sensitivity of VWC prediction to Waxman and Smits parameters as the standard deviation was about 0.03 to 0.014 %. Outside the root zone, VWC values predicted from Waxman and Smits model were consistent with those from retention curve (Fig. 8) suggesting the ability of ER to predict soil moisture in homogenous soil system. Differences in VWC prediction inside the root zone were observed for the wet as well as for the dry state (Fig. 8). Moreover, ER values were smaller than 50 Ωm indicating the limit of Waxman and Smits model as suggested by Laloy et al. (2011). A good consistency between Waxman and Smits and retention curve predictions observed during the wet state highlights the ability of ER to predict soil moisture (Fig. 9). Outside the root zone, a linear relationship was observed between VWC predicted from Waxman and Smits model and retention curve. Inside the root zone, VWC predicted with Waxman and Smits model overestimates soil moisture for the wet as well as for the dry state. Soil moisture overestimation inside the root zone was probably related to soil heterogeneities. Also, shallow groundwater up to 2 m deep maintained a high level of saturation along the toposequence. No change in water content occurred since the all pores of the saturated zone were occupied by water. We conclude that changes in ER were probably related to those in electrical conductivity of soil water. We also observed a high chloride concentration below the hedgerow in the same toposequence (Grimaldi et al., 2009). It is well known that ER decreases when ionic concentration increases (Ward, 1990). Since chloride is a conservative solute, its concentration increased with water and nutrient uptake. At this location, the highly conductive structures (dark blue in Fig. 4) were observed below the hedgerow in agreement with observations of chloride concentration (Grimaldi et al., 2009). These structures, probably due to a high chloride concentration, moved little over time on the ER maps (T01 to T10, Fig. 4). The conductive structure observed at UP1 from T01 to T04 disappeared at T05 due to high rainfall (Figs. 2 and 3). Rainfall events observed between T04 and T05 should have diluted solutes. Another conductive structure below the hedgerow appeared at T07 and at T09, when root water uptake was highest. Change in conductive zones and their small degree of movement was probably related to water fluxes and chloride concentration.

To analyze the relationship between soil ER and individual parameters, further studies are needed. High-resolution analysis should be performed by monitoring chloride concentration, ER, and soil matric potential at the same spatial (grid size) and temporal resolutions. In this way, the perspective of using ER maps as a proxy for chloride accumulation in the vadose zone could be addressed.

The originality of our approach consists on analyzing both spatial and temporal effects of soil moisture. Spatial effect due to the root zone induced a non-stationarity of the relationship between VWC (or ψ) and ER (Figs. 7 and 8). The temporal effect was mainly controlled by the seasonality (wet and the dry periods) which is well known as a first order forcing.

5 Conclusions

ERT monitoring offers a non-invasive tool with a high resolution providing information about soil horizon geometry as well as physical and chemical properties. Geophysical signal can be interpreted by considering the main parameters (i.e. structure, water content, fluid composition) revealing individual contribution but combined effects are more difficult to consider.

The driest zones, below the hedgerow, identified using ER changes and matric potential maps were consistent with vertical and horizontal root density. A dry soil below the hedgerow, with a high matric-potential gradient indicates water flux toward the hedgerow.

The Pdfs of ER and matric potential measurements for wet and dry states show largest difference in mean values in the topsoil layer. Results of ER were consistent with matric potential measurements with two different behaviors for locations inside and outside the root zone. A strong correlation ($r = 0.9$) between VWC values from Waxman and Smits model and those obtained from retention curve was observed outside the root zone. In our case study, a shift of ER and soil moisture relationship was observed between the locations inside and outside the root zone. We assume that, inside the root zone, soil heterogeneities were related to the high root density and also to a particular topographical context (ditch and bank at the hedgerow proximity) which is encountered in Brittany and over north-west of Europe. We hypothesized that soil heterogeneities lead to the shift in the relationship between ER and soil moisture. The non-stationarity in this relationship suggests the combined effects on ER signal which should be corrected by improving data processing. Similar monitoring with ERT should be extended to various transects with contrasted topographical context. More investigations on heterogeneous soil system would help not only to characterize structures

SOILD
2, 955–994, 2015

(soil, weathered bedrock and bedrock) but also to improve temporal and spatial soil moisture prediction. In many hedgerow landscapes where linear vegetation structure is high, heterogeneities in soil system are mainly due to anthropogenic topographical singularities such as ditchs and banks. ER signal deconvolution to separate the effect related to root system from the perturbation due to the singularities require further investigations.

The Supplement related to this article is available online at doi:10.5194/-15-955-2015-supplement.

Acknowledgements. Part of this work was supported by the ECOGER program ACI Ecco. The authors thank INRA and AGROCAMPUS OUEST for supporting this research. The Mogis and Courtillon families kindly accepted the installation of experimental equipment on their fields.

References

Adam, I., Michot, D., Guero, Y., Soubega, B., Moussa, I., Dutin, G., and Walter, C.: Detecting soil salinity changes in irrigated Vertisols by electrical resistivity prospection during a desalinisation experiment, Agricultural and Water Management, 109, 1–10, doi:10.1016/j.agwat.2012.01.017, 2012.

Al Hagrey, S. A.: Geophysical imaging of root-zone, trunk, and moisture heterogeneity, J. Exp. Bot., 58, 839–854, doi:10.1093/jxb/erl237, 2007.

Al Hagrey, S. A. and Michaelsen, J.: Resistivity and percolation study of preferential flow in vadose zone at Bokhost, Germany, Geophysics, 64, 746–753, 1999.

Al Hagrey, S. A. and Petersen, T.: Numerical and experimental mapping of small root zones using optimized surface and borehole resistivity tomography, Geophysics, 76, 25–35, 2011.

Amato, M., Basso, B., Celano, G., Bitella, G., Morelli, G., and Rossi, R.: In situ detection of tree root distribution and biomass by multi-electrode resistivity imaging, Tree Physiol., 28, 1441–1448, 2008.

Amato, M., Bitella, G., Rossi, R., Gómez, J. A., Lovelli, S., and Gomes, J. J. F.: Multi-electrode 3D resistivity imaging of alfalfa root zone, Eur. J. Agron., 31, 213–222, doi:10.1016/j.eja.2009.08.005, 2009.
Archie, G. E.: The electrical resistivity log as an aid in reservoir characteristics, Transactions of the AIME, 146, 54–62, 1942.
Baffet, M.: Influence de la haie sur l'évolution des caractères physico-chimiques et hydrodynamiques des sols, Thèse de doctorat de l'Université de Limoges, 1984.
Beff, L., Günther, T., Vandoorne, B., Couvreur, V., and Javaux, M.: Three-dimensional monitoring of soil water content in a maize field using Electrical Resistivity Tomography, Hydrol. Earth Syst. Sci., 17, 595–609, doi:10.5194/hess-17-595-2013, 2013.
Besson, A., Cousin, I., Samouëlian, A., Boizard, H., and Richard. G.: Structural heterogeneity of the soil tilled layer as characterized by 2D electrical resistivity surveying, Soil Till. Res., 79, 239–249, 2004.
Bréda, N., Granier, A., Barataud, F., and Moyne, C.: Soil-water dynamic in an oak stand. I. Soil moisture, water potentials, and water uptake by roots, Plant Soil, 172, 17–27, 1995.
Brillante, L., Bois, B., Mathieu, O., Bichet, V., Michot, D., and Lévêque, J.: Monitoring soil volume wetness in heterogeneous soils by electrical resistivity. A field-based pedotransfer function, J. Hydrol., 516, 55–66, doi:10.1016/j.jhydrol.2014.01.052, 2014.
Brillante, L., Mathieu, O., Bois, B., van Leeuwen, C., and Lévêque, J.: The use of soil electrical resistivity to monitor plant and soil water relationships in vineyards, SOIL, 1, 273–286, doi:10.5194/soil-1-273-2015, 2015.
Caubel, V.: Influence de la haie de ceinture de fond de vallée sur les transferts d'eau et de nitrate, Thèse de Doctorat de l'Ecole Nationale des Sciences Agronomiques de Rennes, 2001.
Decagon Devices.: Mini disk infiltrometer, Model S, user's manual version3, Decagon devices, Pullman, WA, 2006.
Descloitres, M., Ribolzi, O., Le Troquer, Y., and Thiébaux, J. P.: Study of water tension differences in heterogeneous sandy soils using surface ERT, J. Appl. Geophys., 64, 83–98, 2008.
Drénou, C.: Les racines, face cachée des arbres, Institut pour le développement forestier, Paris, 2006.
FAO: World Reference Base for Soil Resources, IUSS Working Group, 2nd edition FAO, World Soil Resources Report No. 103, FAO, Rome, 2006.

SOILD
2, 955–994, 2015

Ferren, J. C.: Monographie du climat, Station de Rennes-Le Rheu, Analyse sur 30 années des moyennes mensuelles 1971–2000, INRA, Rennes, 2004.

Garré, S., Javaux, M., Vanderborght, J., Pagès, L., and Vereecken, H.: Three-dimensional electrical resistivity tomography to monitor root zone water dynamics, Vadose Zone J., 10, 412–424, 2011.

Garré, S., Günther, T., Diels, J., and Vanderborght, J.: Evaluating experimental design of ERT for soil moisture monitoring in contour hedgerow inter-cropping systems, Vadose Zone J., 11, doi:10.2136/vzj2011.0186, 2012.

Garré, S., Coteur, I., Wongleecharoen, C., Kongkaew, T., Diels, J., and Vanderborght, J.: Noninvasive monitoring of soil water dynamics in mixed cropping systems. A case study in Ratchaburi Province, Thailand, Vadose Zone J., 12, 1–12, doi:10.2136/vzj2012.0129, 2013.

Ghazavi, G., Thomas, Z., Hamon, Y., Marie, J. C., Corson, M., and Merot, P.: Hedgerow impacts on soil-water transfert due to rainfall interception and root-water uptake, Hydrol. Process., 22, 4723–4735, 2008.

Ghazavi, G., Thomas, Z., Hamon, Y., and Merot, P.: Spatial and temporal variation of soil-water movement under a hillslope hedgerow during contrasting meteorological conditions, Hydrol. Process., 25, 1431–1442, 2011.

Grimaldi, C., Thomas, Z., Fossey, M., Fauvel, Y., and Merot, P.: High chloride concentrations in the soil and groundwater under an oak hedge: an indicator of evapotranspiration and water movement, Hydrol. Process., 23, 1865–1873, 2009.

Hadzick, Z. Z., Guber, A. K., Pachepsky, Y. A., and Hill, R. L.: Pedotransfer functions in soil electrical resistivity estimation, Geoderma, 164, 195–202, doi:10.1016/j.geoderma.2011.06.004, 2011.

Hesse, A.: Resistivity prospecting, in: Archaeological prospecting and remote sensing, edited by: Scollar, I., Tabbagh, A., Hesse, A., and Herzog, I., Cambridge University Press, Cambridge, 307–374, 1990.

Laloy, E., Javaux, M., Vanclooster, M., Roisin, C., and Bielders, C. L.: Electrical resistivity in a loamy soil: identification of the appropriate pedo-electrical model, Vadose Zone J., 10, 1023–1033, doi:10.2136/vzj2010.0095, 2011.

Linde, N., Binley, A., Tryggvason, A., Pedersen, L. B., and Revil, A.: Improved hydrogeophysical characterization using joint inversion of crosshole electrical resistance and ground-penetrating radar traveltime data, Water Resour. Res, 42, W12404, doi:10.1029/2006WR005131, 2006.

SOILD
2, 955–994, 2015

Non-stationarity of electrical resistivity and soil moisture relationship

D. Michot et al.

Loke, M. H. and Barker, R. D.: Rapid least-squares inversion of apparent resistivity pseudo-sections by a quasi-Newton method, Geophys. Prospect., 44, 131–152, 1996.

Lucot, E.: Influence des caractéristiques de la piérrosité des sols sur la prospection racinaire et l'alimentation hydrique des arbres. Application à l'estimation de la valeur des sols forestiers, Thèse de doctorat de l'Université de Franche-Comté, 1994.

Michot, D.: Intérêt de la géophysique de subsurface et de la télédétection multispectrale pour la cartographie des sols et le suivi de leur fonctionnement hydrique à l'échelle intraparcellaire, Thèse de l'Université Paris VI, 2003.

Michot, D., Dorigny, A., and Benderitter, Y.: Determination of water flow direction and corn roots-induced drying in an irrigated Beauce CALCISOL, using electrical resistivity measurements, Comptes Rendus De L'Academie Des Sciences Serie II Fascicule a-Sciences De La Terre Et Des Planetes, 332, 29–36, 2001.

Michot, D., Benderitter, Y., Dorigny, A., Nicoullaud, B., King, D., and Tabbagh. A.: Spatial and temporal monitoring of soil water content with an irrigated corn crop cover using surface electrical resistivity tomography, Water Resour. Res., 39, 1138–1158, 2003.

Müller, K., Vanderborght, J., Englert A., Kemna, A., Huisman, J. A., Rings, J., and Vereecken, H.: Imaging and characterization of solute transport during two tracer tests in a shallow aquifer using electrical resistivity tomography and multilevel groundwater samplers, Water Resour. Res, 46, 1–23, W03502, doi:10.1029/2008WR007595, 2010.

Nijland, W., van der Meijde, M., Addink, E. A., and de Jong, S. M.: Detection of soil moisture and vegetation water abstraction in a Mediterranean natural area using electrical resistivity tomography, Catena, 81, 209–216, 2010.

Pride, S.: Governing equations for the coupled electromagnetics and acoustics of porous media, Phys. Rev. B, 50, 15678–15696, doi:10.1103/PhysRevB.50.15678, 1994.

Rossi, R., Amato, M., Bitella, G., Bochicchio R., Ferreira Gomes, J. J., Lovelli, S., Martorella, E., and Favale, P.: Electrical resistivity tomography as a nondestructive method for mapping root biomass in an orchard, Eur. J. Soil Sci., 62, 206–215, doi:10.1111/j.1365-2389.2010.01329.x, 2011.

Samouëlian, A., Cousin, I., Tabbagh A., Bruand, A., and Richard, G.: Electrical resistivity survey in soil science: a review, Soil Till. Res., 83, 173–193, 2005.

Srayeddin, I. and Doussan, C.: Estimation of the spatial variability of root water uptake of maize and sorghum at the field scale by electrical resistivity tomography, Plant Soil, 319, 185–207, 2009.

Thomas, Z., Molénat, J., Caubel, V., Grimaldi, C., and Mérot, P.: Simulating soil-water movement under a hedgerow surrounding a bottomland reveals the importance of transpiration in water balance, Hydrol. Process., 22, 577–585, 2008.
Thomas, Z., Ghazavi, R., Merot, P., and Granier, A.: Modelling and observation of hedgerow transpiration effect on water balance components at the hillslope scale in Brittany, Hydrol. Process., 26, 4001–4014, 2012.
Van Genuchten, M. T.: A Closed-form equation for predicting the hydraulic conductivity of unsaturated soils, Soil Sci. Soc. Am. J., 44, 892–898, 1980.
Walter, C., Mérot, P., Layer, B., and Dutin, G.: The effect of hedgerows on soil organic carbone storage in hillslopes, Soil Use Manage., 19, 201–207, 2003.
Ward, S. H: Resistivity and induced polarization methods, in: Investigations in Geophysics No 5, Geotechnical and Environmental Geophysics, edited by: Ward, S. H., Society of Exploration Geophysicists, Tulsa, Oklahoma, 1990.
Waxman, M. H. and Smits, L. J. M.: Electrical conductivities in oil-bearing shaly sands, Soc. Pet. Eng. J., 8, 107–122, doi:10.2118/1863-A, 1968.
Werban, U., al Hagrey, S. A., and Rabbel, W.: Monitoring of root-zone water content in the laboratory by 2D geoelectrical tomography, J. Plant Nutr. Soil Sci., 171, 927–935, 2008.
Wooding, R. A.: Steady infiltration from a shallow circular pond, Water Resour. Res., 4, 1259–1273, 1968.
Yamakawa, Y., Kosugi, K., Katsura, N., Masaoka, N., and Mizuyama, T.: Spatial and temporal monitoring of water content in weathered granitic bedrock using electrical resistivity imaging, Vadose Zone J., 11, doi:10.2136/vzj2011.0029, 2012.
Zenone, T., Morelli, G., Teobaldelli, M., Fischanger, F., Matteucci, M., Sordini, M., Armani, A., Ferre, C., Chiti, T., and Seufert, G.: Preliminary use of groundpenetrating radar and electrical resistivity tomography to study tree roots in pine forests and poplar plantations, Commonwealth Scientific and Industrial Research Organization, Collingwood, Australia, 2008.
Zhou, Q. Y., Shimada, J., and Sato, A.: Three-dimensional spatial and temporal monitoring of soil water content using electrical resistivity tomography, Water Resour. Res., 37, 273–285, 2001.

SOILD
2, 955–994, 2015

Non-stationarity of electrical resistivity and soil moisture relationship

D. Michot et al.

Table 1. Waxman and Smits parameters used for volumetric water content prediction. 27 simulations were performed.

	a ($S\,m^{-1}$)	b ($S\,m^{-1}$)	n
Value 1	0.059	1.00×10^{-3}	1.0356
Value 2	0.080	1.00×10^{-3}	1.1271
Value 3	0.150	1.00×10^{-3}	1.3996

SOILD
2, 955–994, 2015

Table 2. Statistics of electrical resistivity measurements calculated from the 548 cells of the entire 2-D section (whole domain) at each monitoring time (T01 to T10) of electrical resistivity tomography.

Electrical resistivity (Ωm)	T01	T02	T03	T04	T05	T06	T07	T08	T09	T10
Minimum	9.2	10.5	10.9	11.8	10.6	10.7	11.4	11.7	12.1	9.3
Maximum	615.2	436.3	386.8	493	413.5	382.9	344	354.8	384.1	722.9
SD	63.7	61.6	59.9	63.3	53	52.6	57.2	57	60.6	99.2
Mean	89.2	88.6	86.7	88	78.5	78	80.8	80	83	104.3
Median	74.4	71.9	68.6	68.8	66.4	65.4	64.4	64.7	66.4	73.5

SOILD
2, 955–994, 2015

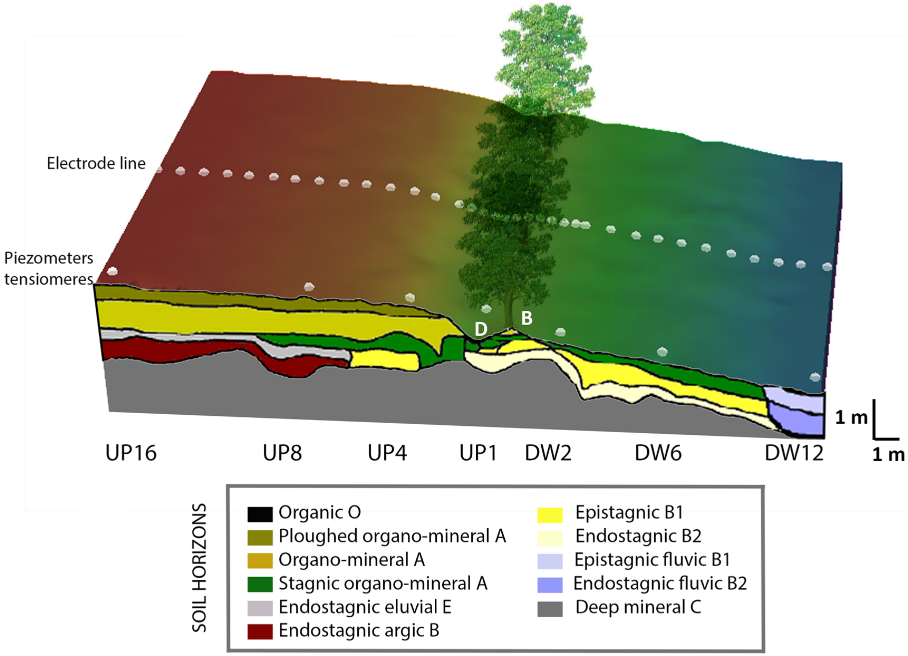

Figure 1. Experimental setup and soil cross section. Soil was excavated up along the toposequence from 16 m upslope (UP16) to 12 m downslope (DW12). Soil horizons are named according to the *World* Reference Base for Soil Resources (FAO, 1998). D and B indicate respectively ditch and bank locations. Each monitored location at UP16, UP8, UP4, UP1, DW2, DW6 and DW12 was equipped with 5 tensiometers and 1 piezometer.

SOILD
2, 955–994, 2015

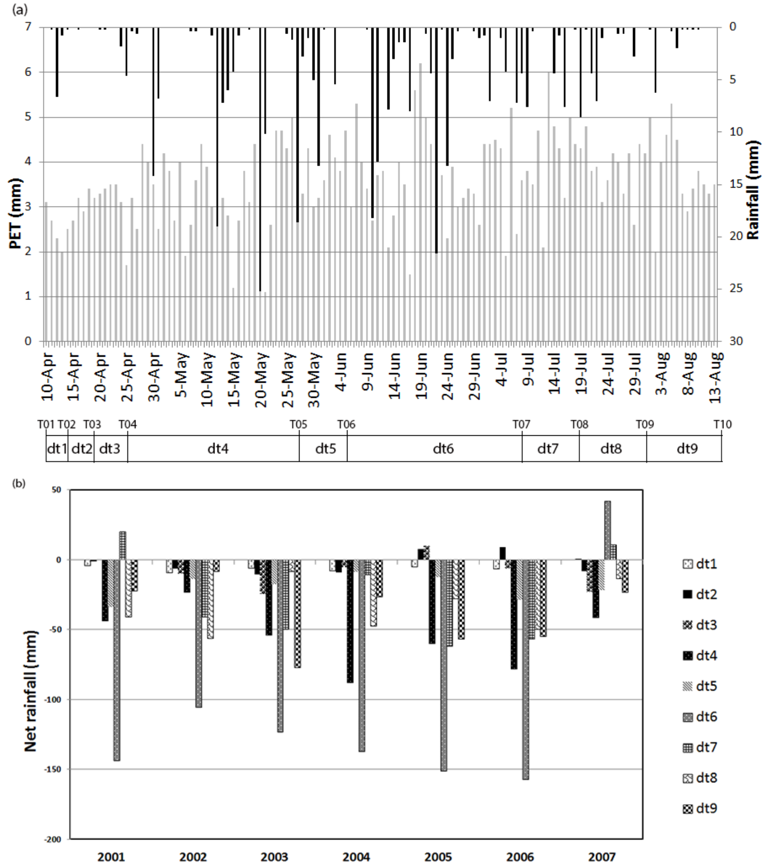

Figure 2. (a) Daily rainfall and potential evapotranspiration (PET) measured during the monitoring period (10 April to 13 August 2007). ERT measurement dates (T01 to T10) and intervals between them (dt1 to dt10) are indicated along the *x* axis. **(b)** Net rainfall (rainfall – PET) calculated for each interval of the monitoring period and compared to those of the previous 6 years.

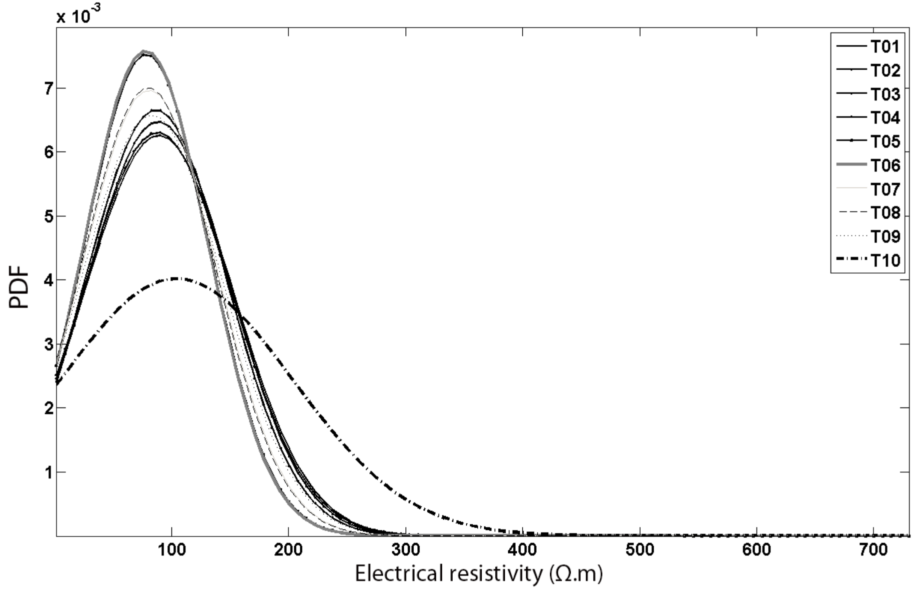

Figure 3. Probability density functions (Pdf) estimated from electrical resistivity measurements of the entire 2-D section at each date of electrical resistivity tomography. Curves were fitted with a Gaussian model.

SOILD

2, 955–994, 2015

Non-stationarity of electrical resistivity and soil moisture relationship

D. Michot et al.

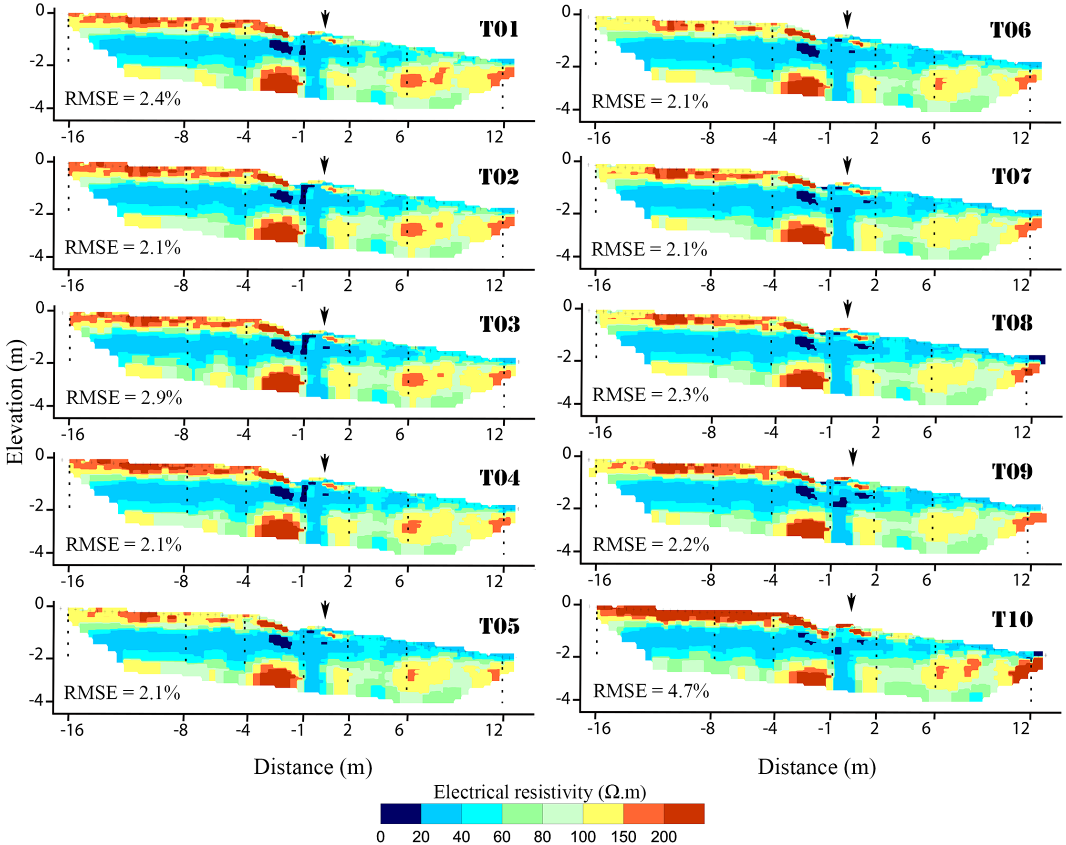

Figure 4. ERT maps at 10 measurement dates (from T01 to T10). Black points indicate tensiometer locations and black arrow the hedgerow location.

SOILD

2, 955–994, 2015

Non-stationarity of electrical resistivity and soil moisture relationship

D. Michot et al.

Title Page
Abstract Introduction
Conclusions References
Tables Figures
◀ ▶
Back Close
Full Screen / Esc
Printer-friendly Version
Interactive Discussion

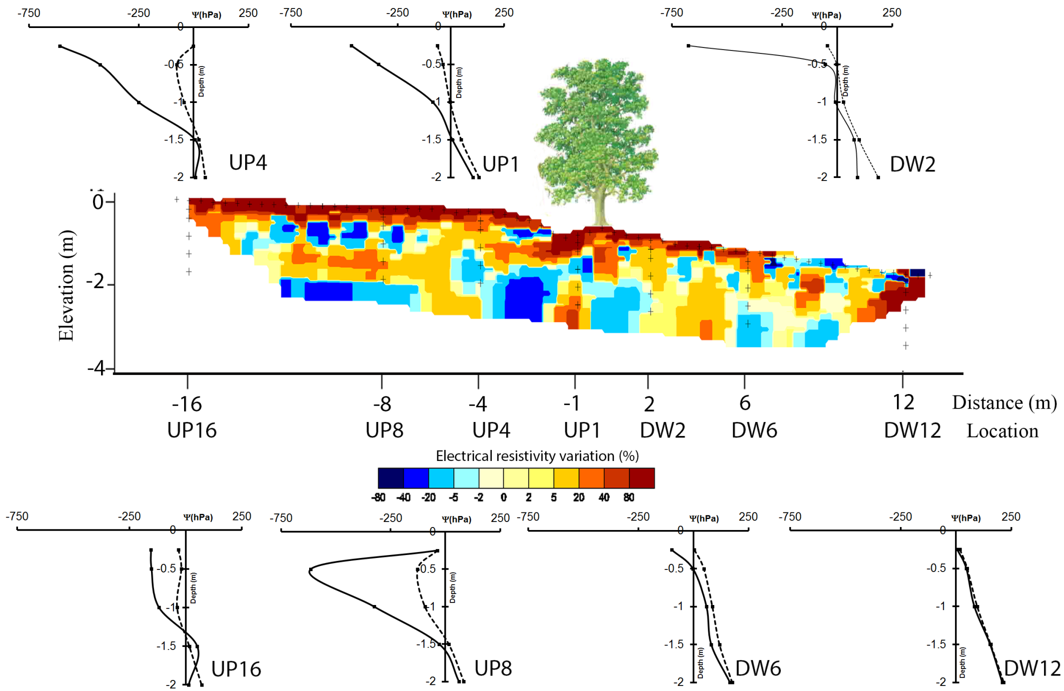

Figure 5. ER variation (%) from initial wet state (T06) to the final dry state (T10) compared to measured soil matric potential profiles. 7 locations i.e. UP16, UP8, UP4 and UP01 for upslope and DW2, DW6 and DW12 for downslope were monitored. The dashed lines indicates the initial wet state and solid lines the final dry state.

SOILD
2, 955–994, 2015

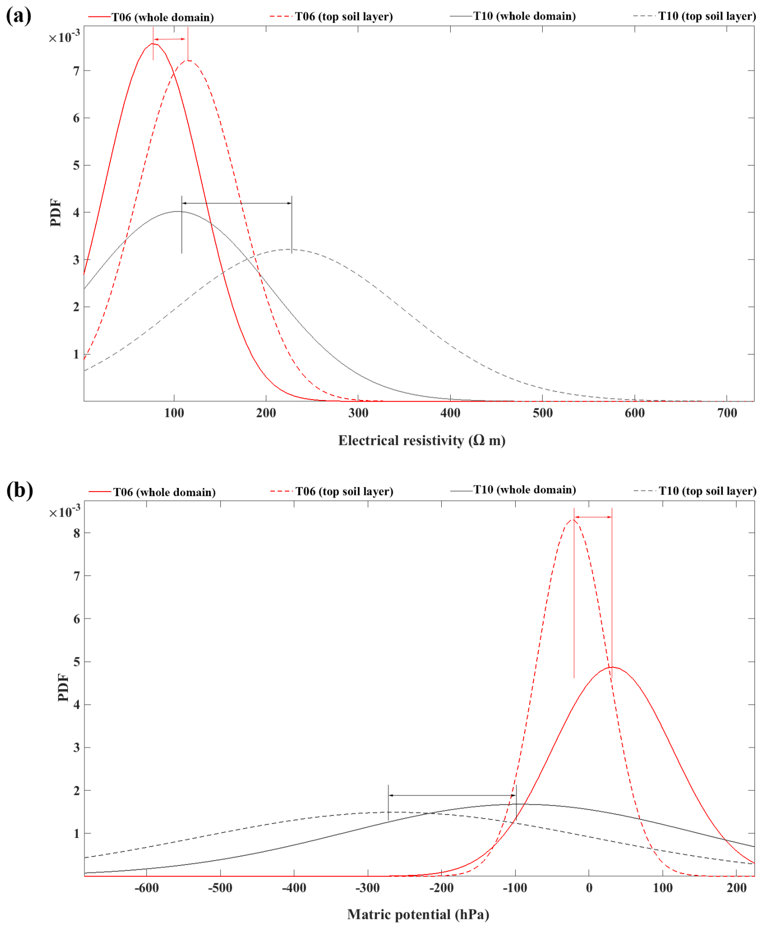

Figure 6. Probability density functions (PDF) of **(a)** electrical resistivity and **(b)** matric potential between wet (T06) and dry (T10) states for the whole domain (solid line) and for the topsoil layer (dash line).

SOILD
2, 955–994, 2015

Non-stationarity of electrical resistivity and soil moisture relationship

D. Michot et al.

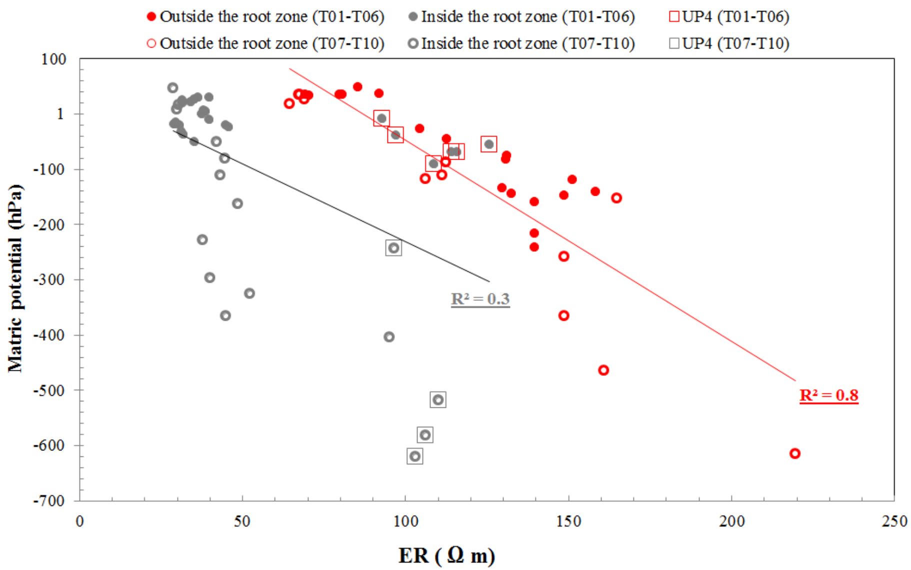

Figure 7. Relationship between matric potential and ER measured in the top soil over the studied period (T01–T10). Red and grey circles indicates all the punctual data respectively outside and inside the root zone. Full circles indicate wet period (T01–T06) and open circles the dry period (T07–T10).

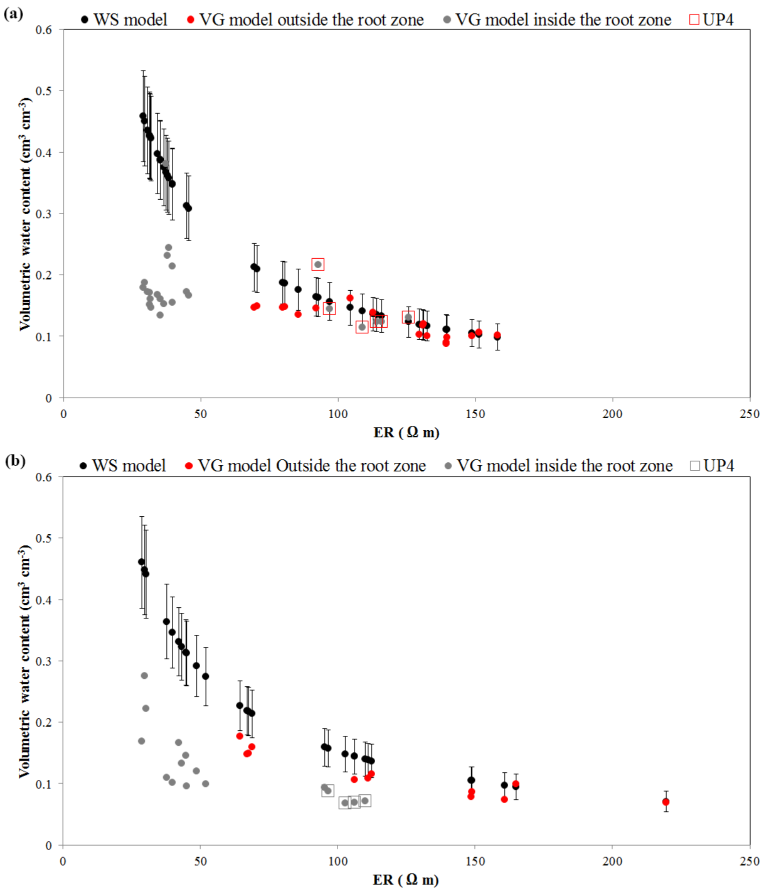

Figure 8. Relationship between VWC and ER in the top soil for the wet period (T01 to T06) **(a)** and the dry period (T07 to T10) **(b)**. Black circles with standard deviation indicate VWC from Waxman and Smits model. Red and grey circles indicate VWC predicted from retention curve respectively outside and inside the root zone.

SOILD
2, 955–994, 2015

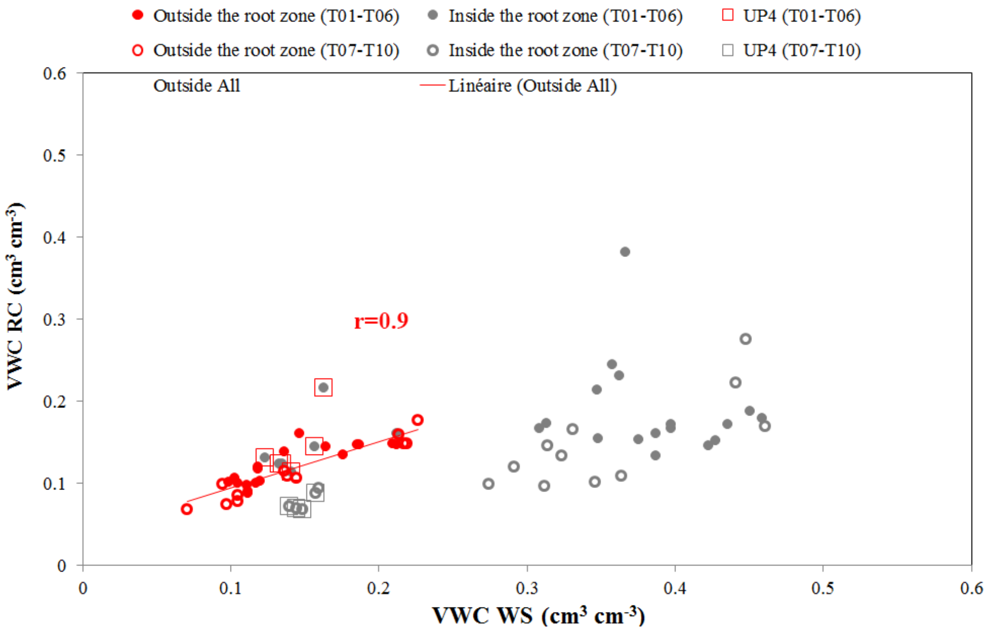

Figure 9. VWC from Waxman and Smits model compared to retention curve prediction outside the root zone (red circles) and inside the root zone (grey circles). The full circles represent the wet period (T01 to T06) and the open circles the dry period (T07–T10).

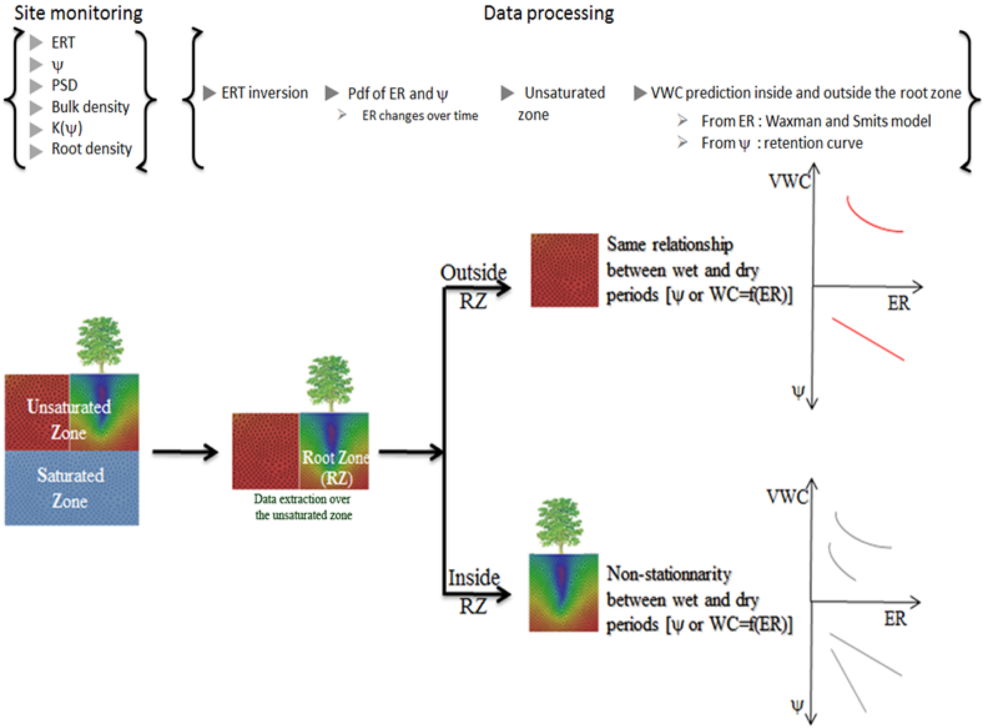

Figure 10. Conceptual scheme summarizing the methodology from site monitoring to data processing.